Journal of Materials Science: Materials in Electronics (2018) 29:11553–11558
https://doi.org/10.1007/s10854-018-9251-5

Investigation on structural, morphology and photoluminescence properties of lanthanum doped zinc oxide nanostructure for optical application by co-precipitation method

C. Selvaraju[1] · N. Athavan[1] · R. Karthick[2]

Received: 7 March 2018 / Accepted: 5 May 2018 / Published online: 10 May 2018

Abstract
The doping of semiconductor by rare earth metal nanoparticles is an effective way for increasing photo catalytic activity. The preparation of ZnO particles with different concentrations of La doping (0, 3, 5 and 7 at.%) via co-precipitation method, and the effects of lanthanum doping concentration on the structures, morphologies and photoluminescence properties were investigated by XRD, FESEM, EDAX and PL. The XRD results indicated that the synthesized La-doped ZnO nanoparticles had the pure wurtzite structure. The crystallite size calculated by Debye–Scherrer's formula is in the range of 36–28 nm. In addition, increasing the doping concentration of La ions in ZnO increase the defects in ZnO lattice and hence resulting in UV emission, which indicate the presence of narrow band-gap in doped nanoparticles.

1 Introduction

Recently rare earth ion doped II–IV semiconductor nanoparticles have received much attention because such doping can modify and improve the optical properties [1–4]. ZnO is an excellent ultraviolet absorber and antibacterial agent. ZnO is one of the metal oxides which attracts due to its direct band gap energy of 3.37 eV and large excitation binding energy of 60 mV. ZnO has wide variety for commercial applications, such as solar cells, field-effect transistors, photo detectors, liquid crystal displays, surface acoustic wave's device, lasers, photo diodes and ultraviolet light emitting diode [5–12].

Doping with rare earth elements leads many interesting properties of ZnO. Usually, semiconducting nanoparticles are known to exhibit exotic physical-chemical properties due to quantum confinement effect. Furthermore, doping with rare earth elements (Ex: La, Tp, Er, Dy and Sm) provides of ZnO materials, which includes the efficient modulation of the emission in the visible range to their unique optical properties. Above all, lanthanum (La)-doped ZnO materials shows excellent gas sensitivity and photo catalytic activity.

In particular, the nanoparticles with smaller size will have larger ratio of surface area to volume, which exhibit the unexpected properties as applied in the visible luminescent devices and excellent photo catalysts [13–15]. Various kinds of fabrication techniques are employed to synthesize ZnO nanoparticles such as thermal decomposition, chemical vapour deposition, sol–gel [16], spray pyrolysis, precipitation [17], vapour phase oxidation and hydrothermal [18]. Among the above techniques, co-precipitation is a promising option for the synthesis and large scale production of ZnO nanoparticles. Moreover, they allow the carry tailoring of synthesis parameters throughout the whole process.

In this paper, we present undoped and La doped, ZnO nanoparticles with various doping concentration via co-precipitation method. The structures, morphological chemical compositions, optical and antibacterial properties of the nanoparticles are discussed in detail.

2 Materials and methods

2.1 Experimental

The La-doped ZnO nanoparticles with various doping concentrations were synthesized by the chemical precipitation route with the starting chemicals of zinc acetate dehydrate,

✉ C. Selvaraju
kcselva2020@gmail.com

[1] PG and Research Department of Physics, H H The Rajah's College (Autonomous), Pudukkottai 622 001, India

[2] PG & Research Department of Physics, National College (Autonomous), Tiruchirappalli 620 001, India

sodium hydroxide, lanthanum nitrate. Zinc acetate dihydrate (0.2 M) was dissolved in de-ionized water with different concentration of La doping (0, 3, 5 and 7 at.%). 0.3 M of NaOH was added drop wise into the obtained solutions until pH attains 8. The solution was continuously stirred and kept at a temperature of 85 °C. The colloidal precipitate obtained was cooled and washed several times with 3:1 ratio of water and ethanol to remove impurities present, if any. The final product was then calculated to 550 °C for 3 h. Method of preparation undoped and La doped ZnO nanoparticles shows in Flowchart 1.

2.2 Characterization

X-ray diffraction (XRD) pattern was recorded at room temperature using PAN analytical X'pert PRO equipment using Cu Kα irradiation as found the wavelength (λ = 1.5418 Å). The morphology of the synthesized powder was examined by FE-SEM (JEOL-JSM-630 FE-SEM) operated at an accelerating voltage, above 5 kV/20 mA and a magnification of 5×10^4. Room temperature photoluminescence (PL) spectral measurements carried out using JY Fluolog 3–11 spectrometer. The elemental composition analysis was made using energy dispersive X-ray analysis (EDAX) (Model: JEOL-JSM 6390 with attachment INCA-penta FETX3 OXFORD).

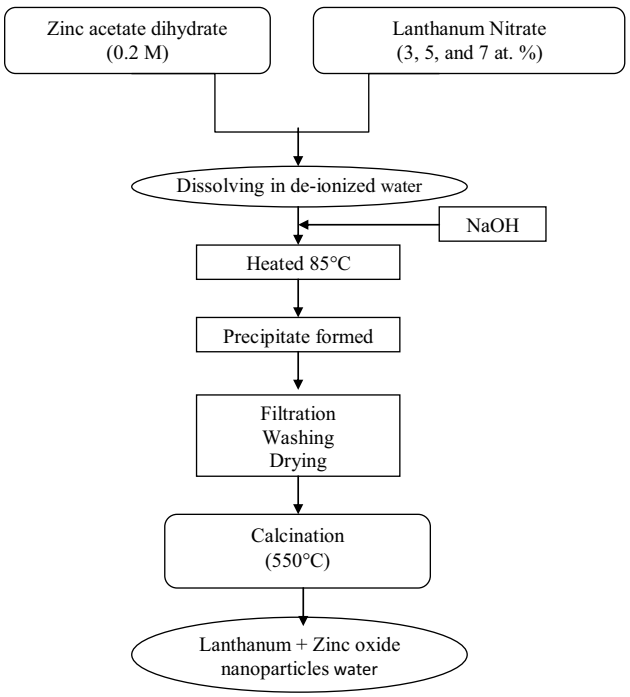

Flowchart 1 The method of preparation undoped and La doped ZnO nanoparticles

2.3 Screening of antibacterial activity

Antibacterial activity test was carried out by agar well diffusion method. Antibacterial activity of the prepared samples was tested in both gram-negative and gram-positive bacteria namely *Staphylococcus aureus* (*S. aureus*) (Gram-positive) and *Escherichia coli* (*E. coli*) (Gram-negative) bacteria using the well diffusion method. The nutrient agar medium was prepared and sterilized by auto clave at 121 °C for 15 min. The medium was poured into the sterile petri plates and allowed to solidity. The bacterial broth culture was webbed on the agar plates using sterile buds and five wells were made by well cutter. After drying, discs were placed in swabbed bacterial plates and incubated at 28 °C for 24 h. After incubation, plates were examined for clear zone around the discs. A clear zone > 2 mm in diameter was taken for antibacterial activity.

3 Results and discussion

3.1 Powder X-ray (XRD) analysis

XRD measurement was employed to investigate the average crystallite size and structural properties of undoped ZnO and La doped ZnO nanoparticles. The diffraction patterns of undoped ZnO and La doped ZnO (0, 3, 5 and 7 at.%) nanoparticles are shown in Fig. 1. The diffraction peaks and their relative intensities of both undoped ZnO and La doped ZnO samples were in good agreement with the standard JCPDS card no. 36-1451. Hence, the observed patterns can be clearly endorsed to the presence of hexagonal wurtzite structure. The XRD peaks for (100), (002) and (101) planes indicate the formation ZnO of phase pure hexagonal wurtzite structure. The high intensity of

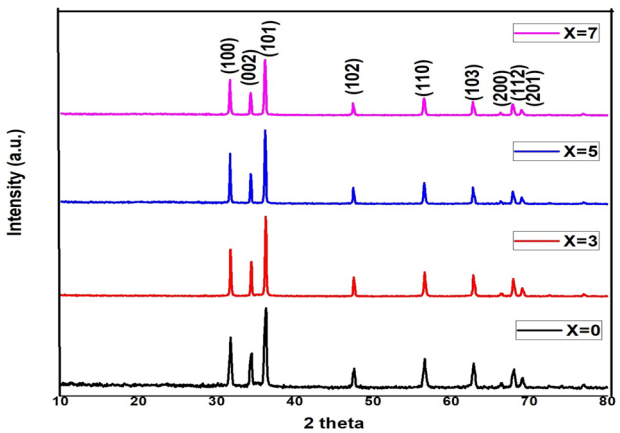

Fig. 1 Powder XRD pattern of La doped ZnO nanoparticles

(101) peak suggests that the growth of nanoparticles has taken place along this direction of crystallization of ZnO. From Fig. 1 no additional XRD peaks were found which clearly indicates the absence of La oxide or Zn–La alloys formation.

The average crystalline size (D) of undoped ZnO and La doped ZnO nanoparticles was determined from the full width at half maximum (FEWHM) by applying to Scherrer's equation [5, 6].

$$D = K\lambda/\beta\cos\theta \quad (1)$$

where β is the FEWHM measured in radiations, θ is the Bragg angle of diffraction, F is the particle shape factor (set to 0.91), λ is the wave length of incident X-ray of 0.1542 nm.

The lattice parameters for a and c for the hexagonal wurtzite structure was evaluated from the (100) and (002) planes, respectively through the following Eqs. [7, 8]:

$$1/d^2_{hkl} = 4/3\left(\frac{h^2+hk+k^2}{a^2}\right) + \left(\frac{l^2}{c^2}\right) \quad (2)$$

Here h, k, l is the miller indices and d_{hkl} represents the interplanar spacing for indices (hkl).

The crystallite sizes of undoped ZnO and La doped ZnO nanoparticles are shown in Table 1, along with the other physical parameters. It can be seen from Table 1 that the crystallite size of La doped ZnO nanoparticles decreased with increase of La present in the samples up to 7%. This observation may be explained by the expansion of ZnO lattice caused by radius of La (1.03 Å) that is layer than that of Zn^{2+} (0.74 Å). Because, La ions substituted with Zn^{2+} ions in the ZnO crystalline structure, the concentration of conduction electrons increases, which leads to the betterment of its certain properties. Moreover, it was clear that La-doping changed the lattice parameters values, but the crystal system (hexagonal) remain unchanged. These results indicate that the lattice constants are not affected much may be the substitution incorporation of La into the O^- sites. The chitosan concentration versus lattice parameter "a" and "c" values plotted in Fig. 2 (Fig. 3) [19].

Table 1 Structural parameters of undoped and La doped ZnO nanoparticles

La doping level (at.%)	D (nm)	Lattice constants[a] (Å)	
		a	c
0	36	3. 220	5.211
3	33	3.256	5. 258
7	31	3. 218	5. 270
6	28	3.260	5.223

[a]Standard values: a = 3.2498 Å, c = 5.2066 Å (JCPDS card no. 36-1451), D—crystallite size

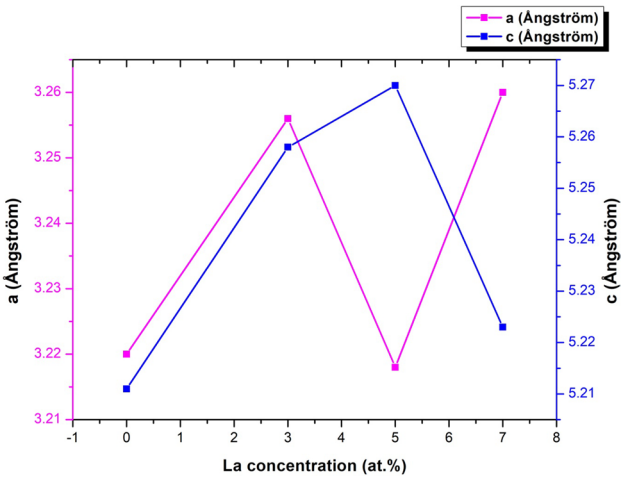

Fig. 2 Variation in the lattice constant versus La doped ZnO nanoparticles

3.2 Morphology and elemental compositions analysis

The FESEM of undoped ZnO and La doped samples are shown in Fig. 3. As can be seen from the images, well defined grains with a perfect hexagonal shape are formed when the La-doping level increased up to 7 at.%. However, the extent of agglomeration is less in the doping system and this is observed and shown in the micrograph for the simultaneously doped samples, well defined nanorods with hexagonal cross section of different lengths and cross sections are visible from these FESEM micrograph. The crystallite size is also evidenced from the TEM image (Fig. 4). From the TEM image, no aggregate observed, in addition, no impurities have been found in ZnO material. The size of these crystalline structures is in the range of ~ 30–70 nm. The EDX results (Fig. 5) showed the presence Zn, O and La by the appearance of their corresponding peaks without any other characteristic peaks and suggested that the prepared do not contain any other element impurities.

3.3 Photoluminescence spectral analysis

The PL spectra are used to study the structural defects and crystalline quality of materials. Figure 6 shows the room temperature PL spectra of undoped ZnO and La doped ZnO nanoparticles. PL spectra of undoped ZnO and La doped ZnO nanoparticles recorded at the excitation wavelength of 325 nm. As shown Fig. 3 the PL spectra samples show prominent peaks at 397, 420 and 467 nm. It is observed that the broad emission in the UV region, centred at (397 nm) is associated with the near band edge emission (NBE) of ZnO results in due to the band to band electronic

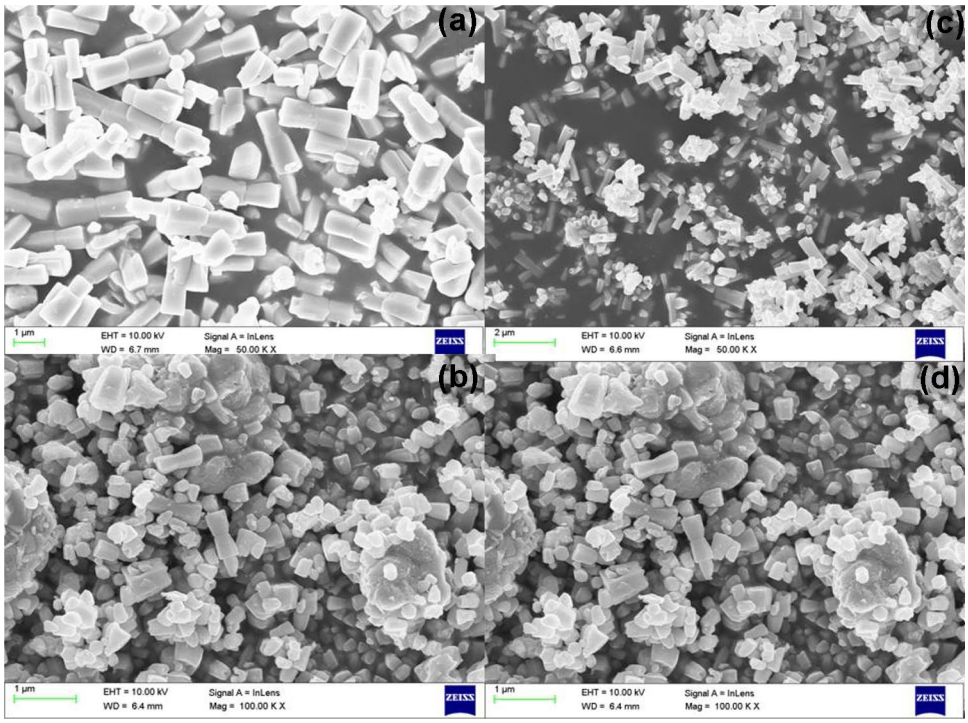

Fig. 3 FESEM images of La doped ZnO **a** 0 at.%, **b** 3 at.%, **c** 5 at.% and **d** 7 at.% nanoparticles

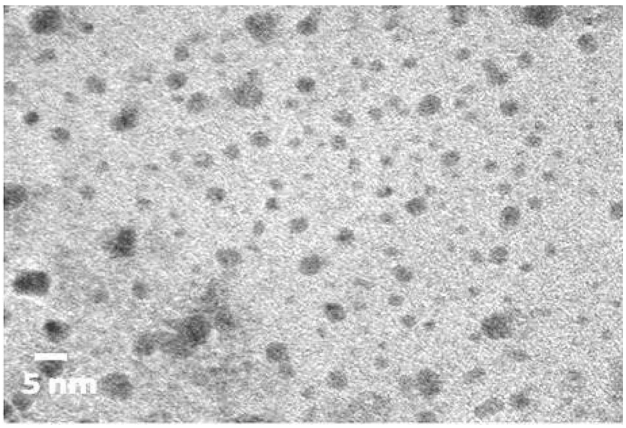

Fig. 4 TEM image of undoped ZnO nanoparticle

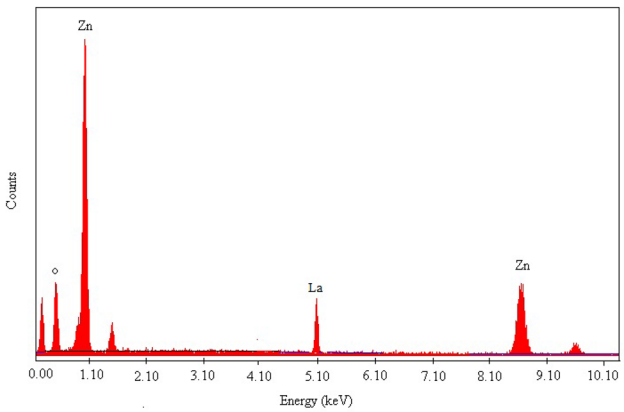

Fig. 5 EDAX spectra of La (7 at.%) doped ZnO nanoparticles

transitions [20]. The strong violet peak at 420 nm is attributed to the recombination of electrons in the zinc interstitial and holes in the valuable band [21]. The peak at 467 nm is associated with the blue emission that originates from the donor level of singly ionized oxygen vacancies to the valance band [22]. This can be also taken as a confirmation that La ion might take part in the substitution of Zn ion and shares the oxygen with Zn atoms [23]. The presence of excess surface defects leads to the stronger blue emission (467 nm) corresponding to the formation of hydroxyl radical [24].

3.4 Antibacterial studies

The antibacterial activity undoped ZnO and La doped ZnO nanoparticles with different concentrations of stock solution was investigated against *S. aureus* (Gram-positive) and *E. coli* (Gram-negative) strains of bacteria using well diffusion method as shown in Fig. 7a, b. The presence of remarkable inhibition zones indicates the good antibacterial efficacy of samples against the microorganism. The zone of inhibition was estimated by measuring the mean diameter around the test sample in mm. The zone inhibition for ZnO against *S. aureus* and *E. coli* bacteria are 21 and 20 mm respectively. For comparison, the variation in the diameter of zone of inhibition is

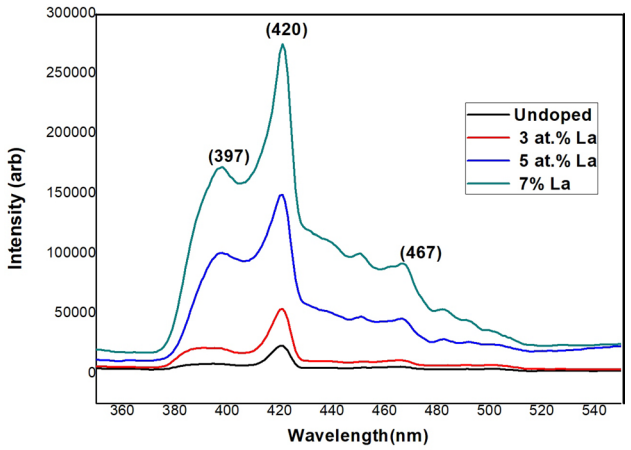

Fig. 6 PL spectra of La doped ZnO nanoparticles

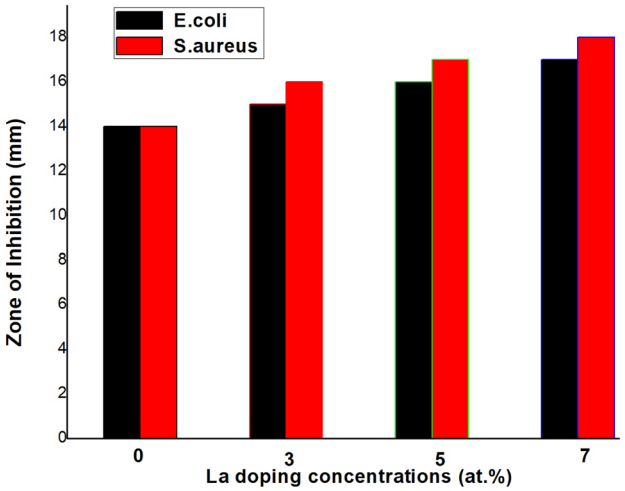

Fig. 8 Variation in the zone of inhibition caused by La doped ZnO nanoparticles

plotted as bar diagram (Fig. 8) for undoped ZnO and La doped ZnO nanoparticles for all two micro-organism. The antibacterial efficacy increases gradually up to doping level of 7 at.% and decrease slightly beyond that doping level. The antibacterial depends jointly on the following parts; (i) the generation of reactive oxygen species (ROS) such as super oxide anion (O_2^-) hydroxyl radical (^-OH) and hydrogen peroxide (H_2O_2), (ii) the size of the grain.

The generation of ROS can be represented as follows [25]:

$$ZnO + h\nu \rightarrow h^+ + e^- \quad (3)$$

$$H^+ + H_2O \rightarrow OH^{\cdot} + H^+ \quad (4)$$

$$O_2 + e^- \rightarrow O_2^{\cdot -} \quad (5)$$

$$O_2^{\cdot -} + H^+ \rightarrow HO_2^{\cdot} \quad (6)$$

$$H^+ + HO_2^{\cdot} + e^- \rightarrow H_2O_2 \quad (7)$$

$$H_2O_2 + O_2^{\cdot -} \rightarrow OH^{\cdot} + O_2 + OH^- \quad (8)$$

From these reactions, it is seen that, the electron hole pairs play a vital role in the generation of ROS. Moreover, as mentioned in the PL studies the peak at 467 nm in the PL spectra of synthesized Zn nanoparticles indicates the presence of singly ionized oxygen vacancies as surface defects. These singly ionized oxygen vacancies induce the formation of hydroxyl radicals on the ZnO surface. As a consequence, the hydroxyl radicals easily penetrate into the call membrane leading to the cell death. Thus, the La (7 at.%) doped ZnO nanoparticles exhibit more antibacterial efficacy for *S. aureus* bacteria and *E. coli* organism.

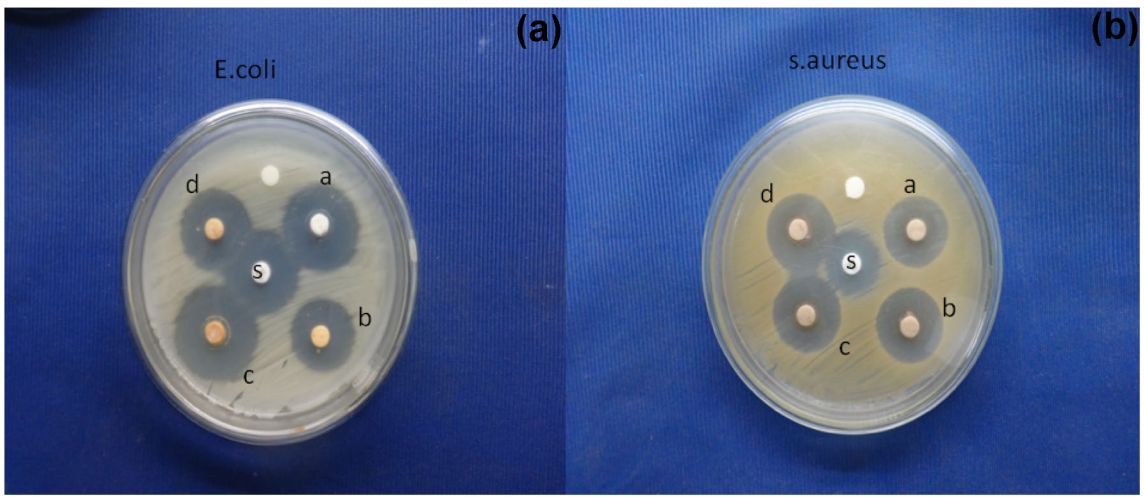

Fig. 7 Antibacterial activity of ZnO:La nanoparticles against **a** *E. coli* and **b** *S. aureus* bacteria

4 Conclusion

The undoped ZnO and La doped ZnO nanoparticles is realized. The structural, morphological and spectroscopic properties are studied and reported. It has been found that the crystalline quality and the average size of crystallite decrease with the increase in the La doping level. The morphological studies by FESEM revealed the formation of nanorods for the undoped ZnO nanoparticles. The NBE peak of the PL spectra confirms the proper substitutional incorporation of La ions O^{2-} sites of the ZnO lattice. The antibacterial studies reveal that the La doping level of 7 at.% is the most studied for the antibacterial activities of La doping ZnO nanoparticles and this antibacterial activity found to be significantly higher for *S. aureus* compared with *E. coli* micro-organism.

References

1. Z. Jia, L. Yue, Y. Zheng, Z. Xu, Mater. Chem. Phys. (2008). https://doi.org/10.1016/j.matcemphys.2007.06.061
2. S.S. Sartiman, N.F. Djaja, R. Saleh, Mater. Sci. Appl. (2013). https://doi.org/10.4236/msa.2013.49065
3. G.A. Prinz, Magnetoeletron. Sci. (1998). https://doi.org/10.1126/Science.282.5394.1660
4. V. Porkalai, D. Benny Anburaj, B. Sathya, G. Nedunchezhian, R. Meenambika, J. Mater. Sci.:Mater. Electron. (2016). https://doi.org/10.1007/s10854-016-5826-1
5. S. Suwanboon, P. Amornpitoksuk, Ceram. Int. **37**, 3515 (2011)
6. C. Ravichandran, G. Srinivasan, C. Lennon, S. Sivananthan, J. Kumar, Superlatt. Microstruct. **49**, 527 (2011)
7. C.-L. Tsai, Y.-J. Lin, C.-J. Liu, L. Horng, Y.-T. Shih, M.-S. Wang, C.-S. Huang, C.-S. Jhang, Y.-H. Chen, H.-C. Chang, Appl. Surf. Sci. **255**, 8643 (2009)
8. S. Anandan, A. Vinu, K.L.P. Sheeja Lovely, N. Gokulakrishnan, P. Srinivasu, T. Mori, V. Murugesan, V. Sivamurugan, K. Ariga, J. Mol. Catal. A **266**, 149 (2007)
9. T. Dhannia, S. Jayalekshmi, M.C.S. Kumar, T.P. Rao, A.C. Bose, J. Phys. Chem. Solids **71**, 1020 (2010)
10. W. Zheng, Q. Miao, Y. Tang, W. Wei, J. Xu, X. Liu, Q. Qian, L. Xiao, B. Huang, Q. Chen, Mater. Lett. **98**, 94 (2013)
11. F. Yakuphanoglu, S. Ilican, M. Caglar, Y. Caglar, Superlatt. Microstruct. **47**, 732 (2010)
12. S. Suwanboon, P. Amornpitoksuk, A. Sukolrat, Ceram. Int. **37**, 1359 (2011)
13. S. Suwanboon, P. Amornpitoksuk, P. Bangrak, N. Muensit, Mater. Sci. Semicond. Proc. **16**, 504 (2013)
14. M.Y. Nassar, M.M. Moustafa, M.M. Taha, RSC Adv. **6**, 42180 (2016)
15. M. Shakir, M. Faraz, M.A. Sherwani, S.I. Al-Resayes, J. Lumin. **76**, 159 (2016)
16. J. Yang, L. Feia, H. Liua, Y. Liu, M. Gaoa, Y. Zhanga, L. Yanga, J. Alloys Compd. **509**, 3672–3676 (2011)
17. Y. Yang, H. Chen, B. Zhao, X. Bao, J. Cryst. Growth **263**, 447–453 (2004)
18. R. Savu, R. Parra, E. Joanni, B. Jancar, S.A. Elizario, R. de Camargo, P.R. Bueno, J.A. Varela, E. Longo, M.A. Zaghate, J. Cryst. Growth **311**, 4102–4108 (2009)
19. G. Magesh, G. Bhoopathi, N. Nithya, A.P. Arun, E. Ranjith Kumar, Superlatt. Microstruct. **117**, 36–45 (2018)
20. M. Ashok kumar, S. Muthukumaran, J. Mag. Mag. Mater. **374**, 61–66 (2015)
21. S. Zhao, Y. Zhou, K. Zhao, Z. Liu, P. Han, S. Wang, W. Xiang, Z. Chen, H. Lu, B. Cheng, G. Yang, Physica B **373**, 154–156 (2006)
22. R. Mariappan, V. Ponnuswamy, P. Suresh, Supperlatt. Microstruct. **52**, 500–513 (2012)
23. T. Prakash, R. Jayaprakash, C. Espro, G. Neri, E. Ranjith Kumar, J. Mater. Sci. **49**, 1776–1784 (2014)
24. N. Talebian, J. Photochem. Photobiol. B **120**, 66–73 (2013)
25. K. Ravichandran, K. Karthika, B. Sakthivel, N. Jabena Begum, S. Snega, K. Swaminathan, V. Senthamilselvi, J. Magn. Magn. Mater. **358**, 50–55 (2014)